# Monte Carlo Simulation of the Heterotypic Aggregation Kinetics of Platelets and Neutrophils

Ian J. Laurenzi and Scott L. Diamond
Institute for Medicine and Engineering, Department of Chemical Engineering, University of Pennsylvania, Philadelphia, Pennsylvania 19104 USA

ABSTRACT The heterotypic aggregation of cell mixtures or colloidal particles such as proteins occurs in a variety of settings such as thrombosis, immunology, cell separations, and diagnostics. Using the set of population balance equations (PBEs) to predict dynamic aggregate size and composition distributions is not feasible. The stochastic algorithm of Gillespie for chemical reactions (Gillespie, 1976. *J. Comput. Phys.* 22:403–434) was reformulated to simulate the kinetic behavior of aggregating systems. The resulting Monte Carlo (MC) algorithm permits exact calculation of the decay rates of monomers and the temporally evolving distribution of sizes and compositions of the aggregates. Moreover, it permits calculation of all moments of these distributions. Using this method, we explored the heterotypic aggregation of fully activated platelets and neutrophils in a linear shear flow of shear rate $G = 335\ s^{-1}$. At plasma concentrations, the half-lives of homotypically aggregating platelet and neutrophil singlets were 8.5 and 2.4 s, respectively. However, for heterotypic aggregation, the half-lives for platelets and neutrophils decreased to 2.0 and 0.11 s, respectively, demonstrating that flowing neutrophils accelerate capture of platelets and growth of aggregates. The required number of calculations per time step of the MC algorithm was typically a small fraction of $\Omega^{1/2}$, where $\Omega$ is the initial number of particles in the system, making this the fastest MC method available. The speed of the algorithm makes feasible the deconvolution of kernels for general biological heterotypic aggregation processes.

## NOMENCLATURE

| | |
|---|---|
| $a(i, j, t)$ | Population-weighted probability of an $i$–$j$ aggregation |
| $A_k$ | Initial concentration of species k |
| $B, b, C$ | Constants in the sum, product, and constant kernels, respectively |
| $c(i, j, t)$ | Probability frequency of an $i$–$j$ aggregation |
| C | Coefficients for efficiency fitting polynomial |
| $F$ | Cumulative volume distribution |
| $G$ | Shear rate |
| $i, j$ | Species indices |
| $k(i, j, t)$ | Second-order rate constant for aggregation |
| $m$ | Number of species in a system |
| $n$ | Volume distribution of particle concentrations |
| $N$ | Particle concentration |
| $N_0$ | Initial monomer concentration |
| $P(\tau, \mu)$ | Aggregation probability density function |
| $P_1(\tau)$ | Probability of an interval of quiescence $\tau$ |
| $P_2(\mu\|\tau)$ | Probability of the $\mu$th aggregation event given an interval of quiescence $\tau$ |
| $\mathcal{P}$ | Volume of an aggregate contributed by platelets |
| $\mathcal{N}$ | Volume of an aggregate contributed by neutrophils |
| $\mathcal{R}$ | The set of real numbers |
| $r_1, r_2$ | Random numbers |
| $s$ | Parametric argument of $\epsilon_{r+h}$ |
| $t$ | Time |
| $T$ | Dimensionless time for the solution of the PBE for the product and constant kernels |
| $u, v$ | Volumes of aggregating particles |
| $u_0$ | Volume of a monomer |
| $u_k$ | Volume of $k$th species |
| $x$ | Volume distribution of particle population |
| $X_i$ | Number of particles of the $i$th species |
| $V$ | Bulk volume |
| $y$ | Volume fraction of platelets |

### Greek letters

| | |
|---|---|
| $\alpha$ | Total aggregation probability density |
| $\beta_G$ | Smoluchowski aggregation kernel |
| $\beta(i, j, t)$ | Coagulation kernel |
| $\delta(u)$ | Dirac's delta function |
| $\delta_{i,j}$ | Kronecker delta function |
| $\phi$ | Dimensionless time for the sum kernel |
| $\epsilon_h$ | Hydrodynamic efficiency of collision |
| $\epsilon_{plat}$ | $\epsilon_{r+h}$ for homotypic platelet aggregation |
| $\epsilon_{plat\text{-}neut}$ | $\epsilon_{r+h}$ for heterotypic platelet-neutrophil aggregation |
| $\epsilon_{neut}$ | $\epsilon_{r+h}$ for homotypic neutrophil aggregation |
| $\epsilon_{r+h}$ | Overall efficiency of aggregation |
| $\epsilon_r$ | Sticking probability (receptor efficiency) |
| $\phi$ | Dimensionless time for the solution of the PBE for the sum kernel |
| $\Gamma(i)$ | Gamma function of argument i |
| $\mu$ | Critical reaction index |
| $\nu$ | Reaction index |
| $\tau$ | Time step and interval of quiescence |
| $\omega$ | Number of particles in a system |
| $\Omega$ | Initial number of particles in bulk |

*Received for publication 9 March 1999 and in final form 1 June 1999.*

Address reprint requests to Dr. Scott L. Diamond, Institute for Medicine and Engineering, Department of Chemical Engineering, University of Pennsylvania, Philadelphia, PA 19104. Tel.: 215-573-5702; Fax: 215-573-2093; E-mail: sld@seas.upenn.edu.



0006-3495/99/09/1733/14 $2.00

## INTRODUCTION

Aggregating cellular or colloidal systems, when studied under defined transport conditions of two- and three-dimensional Brownian diffusion, constant shear rate, or laminar tube flow, can provide important information about the kinetics and strengths of chemical interaction. The Population Balance Equation (PBE) (Smoluchowski, 1917) has been used to predict the size distributions of several homotypic aggregations of biological interest. Among these are platelet aggregation in shear fields (Bell, 1979, 1981; Belval and Hellums, 1986; Bell et al., 1989a,b; Huang and Hellums, 1993a–c; Tandon and Diamond, 1997), neutrophil aggregation in linear shear fields (Taylor et al., 1996; Neelamegham et al., 1997; Tandon and Diamond, 1998), lymphocyte aggregation via 2D Brownian diffusion (Neelamegham and Zygourakis, 1997), rouleaux formation of red blood cells (Samsel and Perelson, 1982), receptor clustering on cell surfaces (Delisi, 1980), and antigen-antibody reactions (Von Schulthess et al., 1983). In an isotropic medium, the discrete form of the PBE describes the temporal change of the concentrations of aggregates composed of $i$ monomers, $N(i, t)$:

$$\frac{\partial N(i,t)}{\partial t} = \frac{1}{2}\sum_{j=1}^{i-1} \beta(j, i-j, t)N(j, t)N(i-j, t) - \sum_{j=1}^{\infty} \beta(i, j, t)N(i, t)N(j, t) \quad (1)$$

The first term on the right-hand side of Eq. 1 represents the generation of $i$-mers by the aggregation of smaller particles. The second term represents consumption of $i$-mers by aggregation with other particles. The coagulation kernel, $\beta(i, j, t)$, contains the probability of an adhesion event between an $i$-mer and a $j$-mer. Although fragmentation of aggregates may be accounted for within this framework, such terms are omitted here. Equation 1 represents a potentially infinite, yet countable set of highly coupled PDEs, inasmuch as there is one equation for each $i$-mer.

Assuming that all aggregation events result from binary collisions, the PBE may be derived by treating all such events as elementary chemical reactions. In this context, the coagulation kernel $\beta(i, j, t)$ is much like a rate constant for an elementary second-order "chemical reaction" between an $i$-mer and a $j$-mer. As we will show, it is proportional to the probability of such a "reaction" occurring. Furthermore, the kernel may be a function of time when particle reactivity increases or decreases in time (e.g., up-regulation or down-regulation of receptors during cellular aggregation). For cellular aggregation, approximate methods are available to make an a priori prediction of $\beta(i, j, t)$ if dynamic receptor stoichiometries and kinetics are known (Bell, 1981; Tandon and Diamond, 1997, 1998; Long et al., 1999).

By treating aggregation as a process akin to chemical reaction, the stochastic formulation of chemical kinetics may be modified to become the mathematical formalism of aggregation, eliminating the need to solve the set of the deterministic PBEs. This is of particular importance in biological and biomolecular aggregation, where the stochastic variation of such events can be significant. Moreover, the stochastic formulation permits a simple description of heterotypic aggregation, such as that of platelets and neutrophils. The aggregation of these cell types (Hamburger and McEver, 1990; Rinder et al., 1991; Evangelista et al., 1996; Konstantopoulos et al., 1998) is relevant to the progression of thrombosis (Bednar et al., 1985; Palabrica et al., 1992; Elizalde et al., 1997; Minamino et al., 1998), unstable angina (Ott et al., 1996), acute myocardial infarction (Neumann et al., 1997), and complications associated with extracorporeal circulation during surgery (Rinder et al., 1992).

We present an efficient Monte Carlo algorithm for simulating both homotypic and heterotypic aggregation processes. The MC algorithm is exact and is limited only by the accuracy of the coagulation kernel, $\beta(i, j, t)$. Furthermore, we show that this method is more efficient than earlier methods (Gillespie, 1975; Shah et al., 1977; Smith and Matsoukas, 1998) in computational speed and data storage, making it the fastest general solution method for heterotypic aggregation to date.

## THEORY

### On the population balance equation

The PBE (Eq. 1) may be derived by treating aggregation as a system of chemical reactions. For example, considering each interaction between an $i$-mer and $j$-mer to be an elementary reaction step, the following equations may be written for monomers, $N(1, t)$ and dimers, $N(2, t)$:

$$\frac{\partial N(1,t)}{\partial t} = -2k(1, 1, t)N(1, t)N(1, t) - \sum_{j=2}^{\infty} k(1, j, t)N(1, t)N(j, t) \quad (2)$$

$$\frac{\partial N(2,t)}{\partial t} = k(1, 1, t)N(1, t)N(1, t) - k(2, 1, t)N(2, t)N(1, t) - 2k(2, 2, t)N(2, t)N(2, t) - \sum_{j=3}^{\infty} k(2, j, t)N(2, t)N(j, t) \quad (3)$$

Although Eqs. 2 and 3 follow directly from the mathematical formalism of chemical kinetics, the discrepancy between them and Eq. 1 is clear. The stoichiometric coefficients of the first term of Eq. 2 and the third term of Eq. 3 do not appear in the PBE. Moreover, the expansion of Eq. 1 for $i = 2$ would place a factor of $\frac{1}{2}$ on the first term of Eq. 3. A general form of the discrete PBE (neglecting fragmenta-

tion) properly accounting for stoichiometry can be written as

$$\frac{\partial N(i,t)}{\partial t} = \frac{1}{2}\sum_{j=1}^{i-1}(1+\delta_{j,i-j})k(j,i-j,t)N(j,t)N(i-j,t) - \sum_{j=1}^{\infty}(1+\delta_{j,i})k(i,j,t)N(i,t)N(j,t) \quad (4)$$

Equation 4 establishes the relationship between the deterministic second-order rate constant $k(i, j, t)$ and the coagulation kernel $\beta(i, j, t)$. That is,

$$\beta(i,j,t) = (1+\delta_{i,j})k(i,j,t) \quad (5)$$

Equation 5 shows that the coagulation kernel $\beta(i, j, t)$ is not the second-order rate constant for the interaction between $i$-mers and $j$-mers, but that they are related. Furthermore, Eq. 5 is true regardless of whether one is characterizing the interaction of $i$-mers and $j$-mers or arbitrary species of indices $i$ and $j$.

Insofar as it accounts for the number of monomers in aggregates, the PBE as expressed in Eq. 1 is limited to describing aggregations of volumetrically monodisperse monomers. A more general form is available, which accounts explicitly for the potentially polydisperse volume distributions of monomers and their aggregates. The continuous PBE describes the time rate of change of the distribution of volumes occupied by aggregates, $n(u, t)$:

$$\frac{\partial n(u,t)}{\partial t} = \frac{1}{2}\int_0^u \beta(v,u-v,t)n(v,t)n(u-v,t)\mathrm{d}v - \int_0^\infty \beta(u,v,t)n(v,t)n(u,t)\mathrm{d}v \quad (6)$$

To compute the concentration of particles with volumes $u$ in a range $(v, v')$, $n(u, t)$ must be integrated as follows:

$$N(v \le u \le v', t) = \int_v^{v'} n(u,t)\mathrm{d}u \quad (7)$$

Therefore, when $n(u, t)$ is a continuous function of particle volume $u$, the concentration of particles with volume exactly equal to $u'$ (i.e., $v = v' = u'$) is zero for all $u'$. This apparent paradox may be resolved by noting that all real systems possess only a finite number of particles. Therefore, $n(u, t)$ cannot be a continuous function because no finite set of particles can occupy the infinite set of volumes in any range $(v, v') \in \mathcal{R}$. In the language of set theory, the set of particles is of a lower *cardinality* than the set of volumes on which they reside. That is, whereas the number of particles and their combinations is only potentially infinite, the number of volumes on any finite range $(v, v')$ is always infinite. Consequently, Eq. 6 is not physically meaningful when $n(u, t)$ is a continuous function of $u$. However, it is more general than Eq. 1, inasmuch as it explicitly permits polydispersity of monomers.

Equation 6 can be solved for finite systems of particles when $n(u, t)$ is a function of Dirac's delta function, circumventing the $N(u, t)$ paradox. This is a consequence of the countability of a discrete set. In this case, $n(u, t)$ will be zero at all but a countable set of particle volumes $u$, and the concentrations of particles of those sizes, $N(u, t)$, may be computed. In aggregations starting with monodisperse monomers at concentration $N_0$, $n(u, 0) = N_0 u_0^{-1}\delta(u/u_0 - 1)$, where $u_0$ is the volume of a monomer. More generally, if the initial particles are polydisperse in volume but occupy a countable set of volumes (such as cells and emulsions), the initial conditions for Eq. 2 would be $n(u, 0) = \Sigma A_k u_k^{-1}\delta(u/u_k - 1)$, where $\{A_k\}$ are the concentrations of particles of volumes $\{u_k\}$ at the beginning of the aggregation. We denote this a *type 1* initial condition. If $u_k = u_0 k$, all particles are initially composed of monodisperse monomers (such as in molecular aggregations), and we denote this a *type 2* initial condition. It is worth noting that type 2 initial conditions always reduce Eq. 6 to Eq. 1. We will use these definitions to distinguish simulations of volumetrically polydisperse and monodisperse cells.

## The aggregation probability density function

As particles aggregate in time, the populations of particles of a given size and composition will change. The instantaneous abundance of different types of particles within a population may be characterized by their joint distribution. For example, the extent of homotypic aggregation may be quantified by a size distribution of the aggregates formed, be it based on particle volume or number of monomers. Likewise, the extent of heterotypic aggregation may be quantified by the joint distribution of the sizes and compositions of the aggregates. In view of the fact that the size-composition distribution defines the state of aggregation, we define a species as a type of aggregate with a specific size and composition.

Species definition is implicit in the PBE. In Eq. 1, $N(i, t)$ represents the concentration of a species with $i$ monomers. Using platelets and neutrophils as an example of heterotypic aggregation, the concentration of a species of particles with $k$ platelets and $l$ neutrophils is $N(k, l, t)$. Alternatively, the formalism of the continuous PBE may be followed, whereby the concentration of a species of aggregate composed of $\mathcal{P}$ fl of platelets and $\mathcal{N}$ fl of neutrophils is defined as $N(\mathcal{P}, \mathcal{N}, t)$. The discretization of volumes may be specified arbitrarily (as in size binning in Coulter counting), as long as the volume distributions of platelet and neutrophil singlets are appropriately represented at the beginning of a simulation. Naturally, the population of a species is restricted to the integers, regardless of how that species is defined.

With the distribution of sizes and compositions of the aggregates defined implicitly by the distribution of species,

the fundamental hypothesis of the stochastic formulation of chemical kinetics may be applied to aggregation phenomena. Reformulating the definition of Gillespie (1977), the average probability at time $t$ that the $i$th and $j$th species will aggregate inside a bulk volume $V$ within the next infinitesimal time interval d$t$ is

$$c(i, j, t)\mathrm{d}t \tag{8}$$

The isolated aggregation probability frequency $c(i, j, t)$ is a species average. For example, fractal densities within porous aggregates, specific topographies, hydrodynamic interactions, and receptor-ligand reactions of a given pair of aggregating particles are treated as their species averages. Moreover, $c(i, j, t)$, like $\beta(i, j, t)$ and $k(i, j, t)$, depends on the relative transport of the two aggregates (diffusion, shear, electrostatic attraction, etc.). Given $X_i$ aggregates of species $i$ and $X_j$ of species $j$ ($j \neq i$), the total number of combinations of species $i$ and $j$ is $X_iX_j$. Thus, the probability at time $t$ that a particle of species $i$ and a particle of species $j$ will aggregate inside $V$ within d$t$ is

$$a(i, j, t)\mathrm{d}t = c(i, j, t)X_iX_j\,\mathrm{d}t \tag{9}$$

Moreover, if two particles of the same species aggregate, the number of combinations is $X_i(X_i - 1)/2!$. Thus, for like interactions, the probability that two particles of species $i$ will aggregate inside $V$ within d$t$ is

$$a(i, i, t)\mathrm{d}t = \tfrac{1}{2}c(i, i, t)X_i(X_i - 1)\mathrm{d}t \tag{10}$$

A system of $m$ species can have at most $m$ like interactions and $m(m - 1)/2!$ unlike interactions, for a total of $m(m + 1)/2$ interactions. To simplify the reaction accounting, we define an index $v$ for each $i, j$ pair that may react ($v \in [1, m(m + 1)/2]$). The set $\{v\}$ defines the total "aggregation space" of the mixture, whose size is equal to the total number of possible interactions. With this set defined, one can determine the probability $\mathrm{P}(\tau, \mu)\mathrm{d}\tau$, that given a state $\{X_i\}$ at time $t$, the next aggregation event will occur within the time interval $(t + \tau, t + \tau + \mathrm{d}\tau)$ and will be the $\mu$th reaction in $\{v\}$. $\mathrm{P}(\tau, \mu)$ is the "aggregation probability density function." Gillespie (1976) has rigorously derived this probability function for a system of $m$ species as

$$\mathrm{P}(\tau, \mu) = a_\mu \exp\left(-\sum_{v=1}^{m(m+1)/2} a_v\tau\right)$$

$$\tau \in [0, 00], \quad \mu \in [1, m(m + 1)/2] \tag{11}$$

## The stochastic aggregation algorithm

The aggregation probability density function $\mathrm{P}(\tau, \mu)$ is the basis of the stochastic simulation algorithm. However, to stochastically generate both $\mu$ and $\tau$, two random numbers must be generated. Consequently, Eq. 11 must be turned into two probability functions that generate $\mu$ and $\tau$ separately. Using the fact that a $p$-fold probability distribution gives the probability of the union of $p$ events, the definition of conditional probability can be invoked, giving

$$\mathrm{P}(\tau, \mu) \equiv \mathrm{P}(\tau \cap \mu) = \mathrm{P}_1(\tau)\mathrm{P}_2(\mu|\tau) \tag{12}$$

The restriction to two-body aggregation events causes the set of all possible aggregation events to be mutually exclusive. Thus $\mathrm{P}_1(\tau)$ may be determined by summing over all possible aggregation types:

$$\mathrm{P}_1(\tau) = \sum_{\mu=1}^{m(m+1)/2} \mathrm{P}(\tau, \mu) = \alpha \exp(-\alpha\tau) \tag{13}$$

$$\alpha = \sum_{\mu=1}^{m(m+1)/2} a_\mu \tag{14}$$

$\mathrm{P}_1(\tau)$ is the probability that an aggregation event will take place in the interval $(t, t + \tau)$, regardless of its type. $\alpha$ is the total aggregation probability frequency, defined as the change in probability of an aggregation event taking place inside the bulk volume $V$ per infinitesimal time segment d$t$.

Subsequently, the probability of a particular type of aggregation given an interval $(t, t + \tau)$ is given as

$$\mathrm{P}_2(\mu|\tau) = a_\mu/\alpha \tag{15}$$

The nature of Eq. 11 is elucidated when expressed through Eqs. 12–15. Eq. 13 shows that the probability of an aggregation event in time follows the exponential distribution, a characteristic of a process in which events occur randomly in time. Equation 15 demonstrates that the particular type of aggregation occurs randomly, depending only on its relative probability of occurring.

Equation 13 gives the probability distribution through which a Monte Carlo algorithm may stochastically determine the time step $\tau$. A random number, $r_1$, generated on the interval [0, 1], is taken as the probability of a reaction in the time period $\tau$ according to $\mathrm{P}_1(\tau)$. As Eq. 13 is a continuous distribution on $\tau$, it must be integrated over $\tau$ to give the probability of an aggregation within $t$ and $t + \tau$:

$$r_1 = \int_0^\tau \mathrm{P}_1(\tau^*)\mathrm{d}\tau^* = \int_0^\tau \alpha \exp(-\alpha\tau^*)\mathrm{d}\tau^* = 1 - \exp(-\alpha\tau) \tag{16}$$

Noting that $1 - r_1$ is stochastically equivalent to $r_1$, the time step $\tau$ as defined in Eq. 16 may be calculated as

$$\tau = \frac{1}{\alpha}\ln\left(\frac{1}{r_1}\right) \tag{17}$$

The reaction number $\mu$ may be determined in a similar way. However, since Eq. 15 is a discrete distribution, $\mu$ must be selected by summing the probabilities $\mathrm{P}_2(v|\tau)$ over $v$ until the addition of the $\mu$th probability exceeds a random number $r_2 \in [0, 1]$. That is, the $\mu$th reaction must be

selected, using the following inequality (Gillespie, 1976):

$$\sum_{\nu=1}^{\mu-1} a_\nu < r_2\alpha \leq \sum_{\nu=1}^{\mu} a_\nu \tag{18}$$

Although Eq. 18 follows directly from the mathematical formulation, it should be noted that inasmuch as $\{a_\nu\}$ rather than $\{c_\nu\}$ is used in the selection process, Eq. 18 weights the reaction probability on both the population levels and the average aggregation probability between a pair of aggregates. That is, fast aggregations and those with more abundant reactants are more likely to occur because they contribute the most to $\alpha$. Equation 18 naturally and rigorously balances the kinetics of rare fast aggregations and slow abundant aggregations.

Fig. 1 outlines the Monte Carlo algorithm. First, the initial distribution of species is given as a type 1 or type 2 initial condition, whereby each species $i$ is defined by a platelet volume $\mathcal{P}$ and neutrophil volume $\mathcal{N}$. After all reaction probabilities $c(i, j, t)$ and total reaction probability $\alpha$ are calculated, two random numbers $r_1$ and $r_2$ are generated. From these, the time step $\tau$ and aggregation event $\mu$ are determined using Eqs. 17 and 18. If the product species $k$ is new, its properties are calculated from those of the reactant species, and $c(k, l, t)$ are calculated for all $l \in [1, k]$. Last, species populations are adjusted, $\alpha$ is recalculated, and the time is updated by $\tau$. The process continues until a prespecified time is reached or until all particles coalesce, at which point $\alpha = 0$. Although we have used the heterotypic aggregation of platelets and neutrophils as an example of binary heteroaggregation, this algorithm is general for aggregations of particles of arbitrarily complex composition by binary collisions.

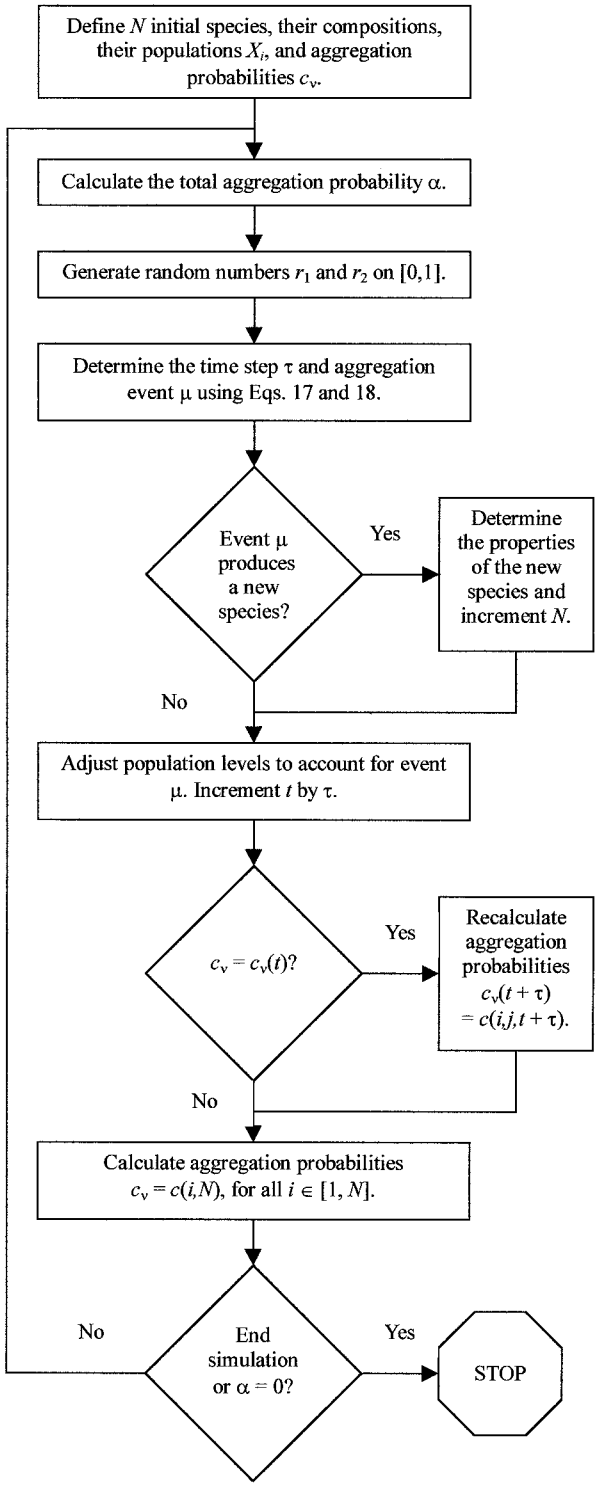


FIGURE 1 The stochastic aggregation algorithm for homotypic and heterotypic aggregations of species with time-dependent reactivities.

## On the relationship of $\beta(i, j, t)$ to $c(i, j, t)$

The coagulation kernel $\beta(i, j, t)$ is intimately related to the isolated aggregation probability frequency $c(i, j, t)$. The average rate of aggregation per unit volume is the bridge through which the two may be related. According to Eq. 9, the average rate of aggregation between species $i$ and $j$ ($i \neq j$) per unit volume is $\overline{c(i, j, t)X_iX_j}/V = c(i, j, t)\overline{X_iX_j}/V$, where again, $V$ represents the bulk volume. According to the deterministic formulation of kinetics, this quantity is $k(i, j, t)N(i, t)N(j, t)$. Noting that the concentrations and populations of species $i$ and $j$ are related by $N(i, t) = \bar{X}_i/V$ and $N(j, t) = \bar{X}_j/V$, the relationship between $k(i, j, t)$ and $c(i, j, t)$ is ($i \neq j$)

$$k(i, j, t) = \frac{\overline{X_iX_j}}{\bar{X}_i\bar{X}_j} Vc(i, j, t) \approx Vc(i, j, t) \tag{19}$$

Likewise, for aggregation between particles of the same species, the average aggregation rate per unit volume is $\frac{1}{2}\overline{c(i, i, t)X_i(X_i - 1)}/V = \frac{1}{2}\overline{c(i, i, t)X_i(X_i - 1)}/V$. Because the deterministic formulation does not change for like aggregation, the relationship between $k(i, i, t)$ and $c(i, i, t)$ is

$$k(i, i, t) = \frac{\frac{1}{2}\overline{X_i(X_i - 1)}}{\bar{X}_i\bar{X}_i} Vc(i, i, t) \approx \frac{1}{2} Vc(i, i, t) \tag{20}$$

Equations 19 and 20 show that $c(i, j, t) \approx (1 + \delta_{ij})k(i, j, t)/V$, a relationship established for chemical reactants (Gillespie, 1976). Considering Eq. 5, the relationship between the aggregation probability frequency $c(i, j, t)$, the coagulation kernel $\beta(i, j, t)$, and the deterministic second-order rate constant $k(i, j, t)$ is

$$c(i, j, t) = \frac{\beta(i, j, t)}{V} \approx \frac{(1 + \delta_{ij})k(i, j, t)}{V} \tag{21}$$

Thus, when aggregations are simulated, where $\beta(i, j, t)$ is known (from experiment, for example), Eq. 21 should be used to find $c(i, j, t)$. Consideration of Eqs. 21 and 9 shows that $\beta(i, j, t)$ is the average probability at time $t$ that the $i$th and $j$th species will aggregate inside any bulk volume per infinitesimal time interval d$t$.

Consideration of Eq. 21 explains the underlying mathematics of Eqs. 1, 5, and 6. When $j \neq i/2$ in Eq. 1 (or $v \neq u/2$ in Eq. 2), the factor of $\frac{1}{2}$ serves to prevent double counting. However, when $j = i/2$ (or $v = u/2$), the factor of $\frac{1}{2}$ is a consequence of the combinations of species. Equations 1 and 6 are deterministic equations based on a stochastic foundation. Based upon the preceding arguments, they may be written as

$$\frac{\partial \bar{X}(i, t)}{\partial t} = \tfrac{1}{2} \sum_{j=1}^{i-1} c(j, i - j, t)\bar{X}(j, t)\bar{X}(i - j, t) - \sum_{j=1}^{\infty} c(i, j, t)\bar{X}(i, t)\bar{X}(j, t) \tag{22}$$

$$\frac{\partial \bar{x}(u, t)}{\partial t} = \tfrac{1}{2} \int_0^u c(v, u - v, t)\bar{x}(v, t)\bar{x}(u - v, t)\mathrm{d}v - \int_0^{\infty} c(u, v, t)\bar{x}(v, t)\bar{x}(u, t)\mathrm{d}v \tag{23}$$

In these equations, $\bar{x}(u, t)$ is the volume distribution of particle population, the analog of $n(u, t)$ for concentration. These are the discrete and continuous forms of the PBE, derived independently by Gillespie (1972) and Ramkrishna (1973).

Equations 22 and 23 only predict properties of the mean behavior of an aggregation. Furthermore, there are implicit assumptions regarding the equality of the products of averages and averages of products. Thus, the stochastic aggregation algorithm is more exact than the PBE, because it does not predict the approximate mean properties of a set of experiments but the properties of a single experiment, and the assumptions regarding averages are circumvented. The average results of an experiment and its moments may be computed from the results from several MC simulations. These moments correspond to those statistical moments of experimental data. The statistics that follow from the simulated aggregations allow one to predict the measured variation in experimental data.

## RESULTS

### Simulation of ideal kernels

Three aggregations with simple kernels $\beta(i, j, t)$ were simulated by MC and compared with analytical solutions of the PBE. Using the methods of Scott (1965), the concentrations of $i$-mers for the sum kernel, product kernel, and constant kernel were analytically calculated with monodisperse initial conditions for the purpose of comparing the results of the stochastic aggregation algorithm with the PBE.

The sum kernel is defined as $\beta(u, v) = B(u + v)$, where $B$ is a constant. Solution of the PBE (Eq. 1 or 6) gives the concentration of $i$-mers $N(i, \phi)$ as

$$N(i, \phi) = N_0(1 - \phi)\frac{(i\phi)^{i-1}}{\Gamma(i + 1)} \exp(-i\phi) \quad \text{for } \phi = 1 - \exp(-BN_0u_0t) \tag{24}$$

where $N_0$ is the initial concentration of monomers and $u_0$ is the volume of a monomer. The discrete solution is a consequence of the monodisperse type 2 initial condition. Likewise, for the product kernel, where $\beta(u, v) = b(uv)$, and $b$ is a constant, the analytical solution for the concentration of $i$-mers is

$$N(i, T) = N_0 \frac{(iT)^{i-1}}{i\Gamma(i + 1)} \exp(-iT) \quad \text{for } T = bN_0u_0^2t \tag{25}$$

Last, the constant kernel ($\beta(u, v) = C = \text{constant}$) has an analytical solution of the form

$$N(i, T) = 4N_0\frac{(T)^{i-1}}{(T + 2)^{i+1}} \quad \text{for } T = CN_0t \tag{26}$$

As Fig. 2 shows, simulations of 10,000 monomers yielded the same results as the analytical solutions of the PBE. The small variation observed is the stochastic noise one would observe experimentally in systems described by these kernels.

### Heterotypic aggregation of platelets and neutrophils in a linear shear field

The heterotypic aggregation of platelets and neutrophils by shear flow represents a complex and important biological system (Rinder et al., 1991; Ott et al., 1996; Konstantopolous et al., 1998; Brown et al., 1998) for demonstrating the stochastic aggregation algorithm. Assuming no hydrodynamic interactions between particles (i.e., linear trajectories), the kernel for orthokinetic aggregation is (Smoluchowski, 1917)

$$\beta_G(u, v) = \frac{G}{\pi}(u^{1/3} + v^{1/3})^3 \tag{27}$$

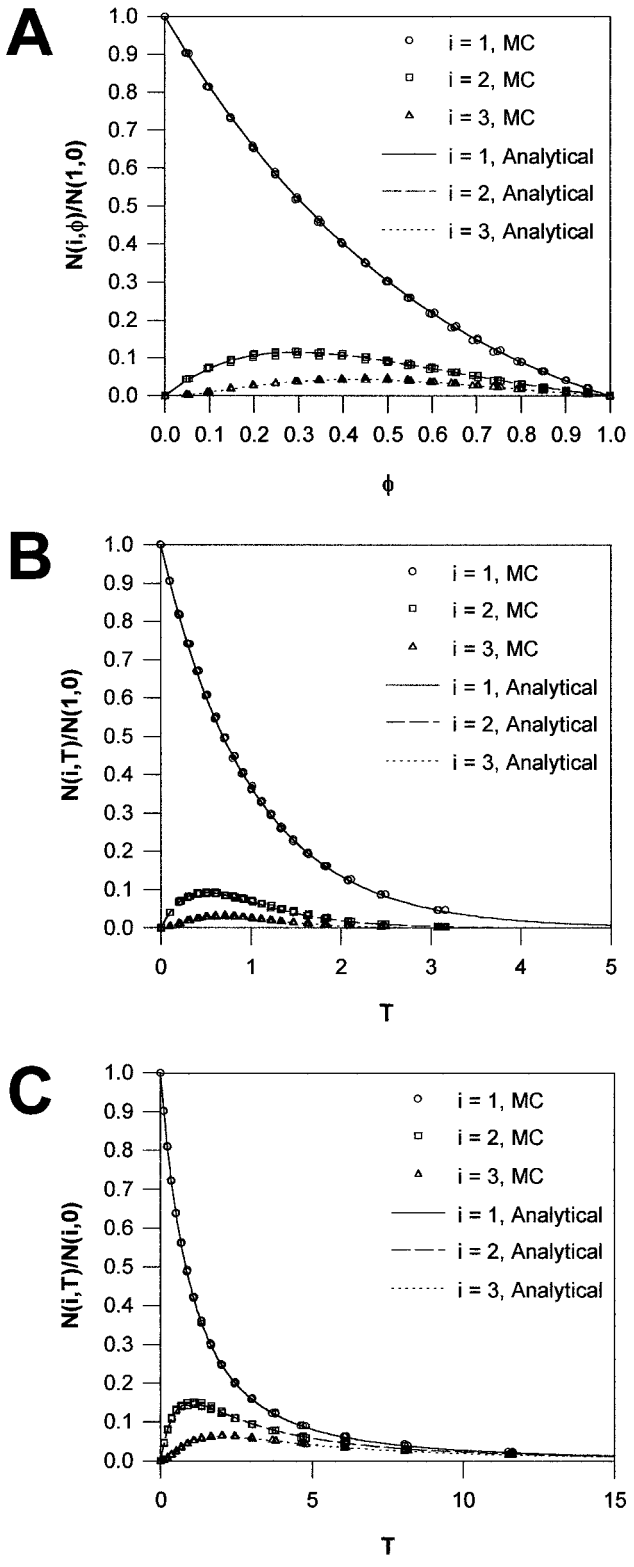


FIGURE 2 Time courses of aggregation for systems modeled by the sum kernel $\beta(u, v) = B(u + v)$ (*A*), product kernel $\beta(u, v) = b(uv)$ (*B*), and constant kernel $\beta(u, v) = C$ (*C*). The kernel is related to the probability of two particles of volumes $u$ and $v$ colliding and successfully aggregating. The solid lines are the analytical solutions of the PBE. Both the PBE and the MC simulation were performed for volumetrically monodisperse monomers and monodisperse initial conditions. In *A*, $N(i, \phi)$ represents the concentration of $i$-mers aggregating by the sum kernel, where $\phi$ is related to time by the relation $\phi = 1 - \exp(-BN_0u_0t)$, $u_0$ is the volume of a monomer, and $N_0$ is the initial number of monomers. The product kernel is represented in *B*, where $N(i, T)$ is the concentration of $i$-mers, and $T = bN_0u_0^2t$. Last, the time course of aggregation of a system described by the constant kernel is displayed in *C*, where $T = CN_0t$.

The Smoluchowski kernel can be corrected for 1) hydrodynamic interactions between particles following curvilinear trajectories and 2) receptor bonding kinetics by introducing two factors, $\epsilon_h$ and $\epsilon_r$ (Tandon and Diamond, 1997, 1998):

$$\beta(u, v) = \epsilon_r\epsilon_h\beta_G(u, v) = \epsilon_{r+h}\beta_G(u, v) \qquad (28)$$

These factors have probabilistic significance. The product of the hydrodynamic efficiency $\epsilon_h$ and $(\beta_G(u, v)/V)d\tau$ is the probability of a collision of two particles of volumes $u$ and $v$ in time $d\tau$. The probability that the two particles stick together upon collision is $\epsilon_r$, termed the *receptor efficiency*. The overall efficiency, $\epsilon_{r+h}$, has been determined experimentally for homotypic aggregations. Partly because of the difficulty of deconvolution of size-composition data, experimentally determined $\epsilon_{r+h}$ are not yet available for heterotypic biological aggregation.

Two types of MC simulations were performed. The first of these was analogous to a solution of the PBE with a type 1 initial condition, allowing for polydispersity in the initial singlet volume of each cell type. Consequently, species were defined as aggregates with specific volumes of platelet and neutrophil content as discussed previously. To obtain physiological initial conditions, human platelets and neutrophils were obtained from healthy donors, isolated, suspended in isotonic buffer, and analyzed using a Coulter counter to obtain their volume distributions. The initial conditions used in the simulations are given in Fig. 6 *A*. The second type of simulation utilized a type 2 initial condition, whereby species were defined as aggregates with specific numbers of volumetrically monodisperse platelets and neutrophils. Singlet volumes were taken as the population means of the aforementioned Coulter distributions: 7.682 fl for platelets and 290.1 fl for neutrophils. All simulations were performed at typical plasma concentrations of platelets and neutrophils: 300,000/$\mu$l and 5,000/$\mu$l, respectively. Because of the available measurement of $\epsilon_{r+h}$ for homotypic platelet aggregation (Bell et al., 1989a,b), simulations were performed at a shear rate $G = 335\ s^{-1}$.

In Fig. 3 we present the results of four MC simulations of homotypic aggregation of platelets, using $\epsilon_{r+h} = 0.05$ (Bell et al., 1989a,b). Simulations were performed with an initial population of 12,000 singlets. In Fig. 3 *A*, the time course of the aggregation is shown for both type 1 and type 2 simulations. Because of the fact that singlets in a type 1 simulation occupied ~90 species, in contrast to one species in a type 2 simulation, the aggregation spaces of the two types of simulation are quite different. However, there was only a 5–6% difference in the fraction of singlets aggregated between the two types of simulation. Maximally activated

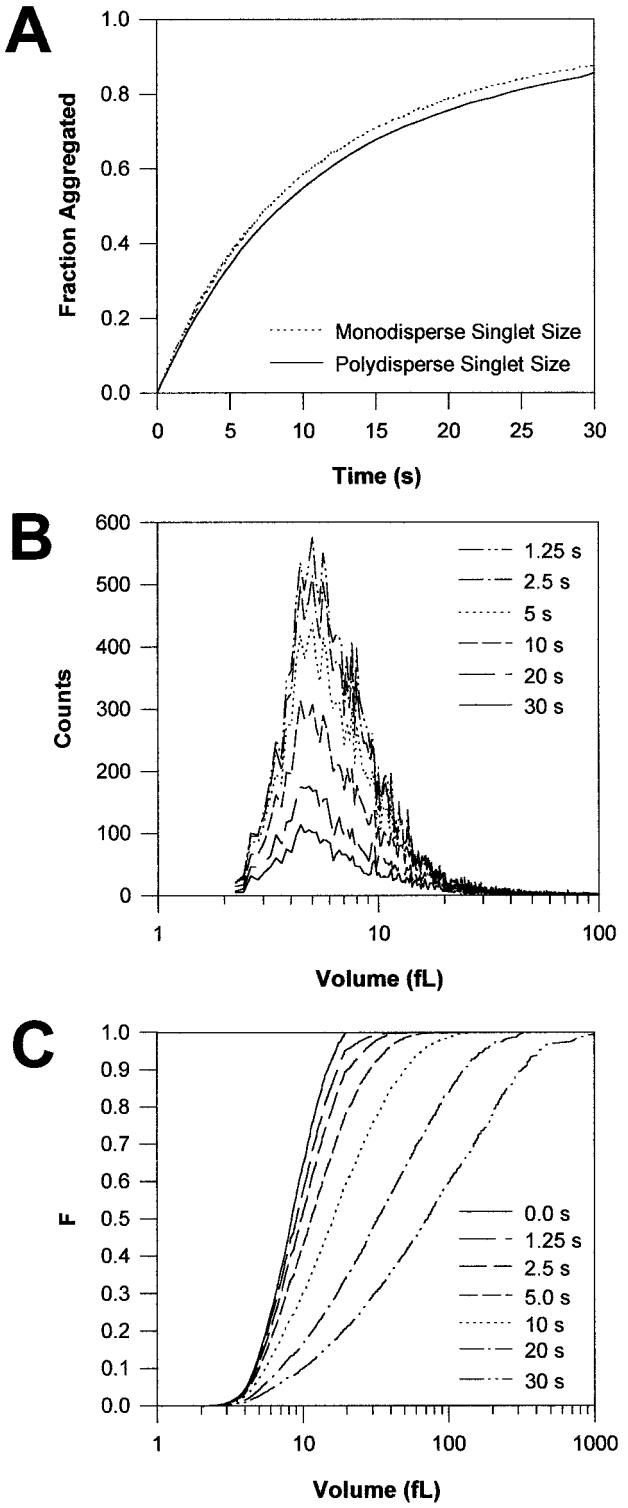


FIGURE 3 Behavior of the homotypic aggregation of fully activated platelets in a linear flow field of 335 $s^{-1}$ ($\epsilon_{r+h}$ = 0.05 for 50,000 CD41/CD61/platelet and 3 mg/ml fibrinogen). The average of four MC simulations (12,000 platelets/simulation) is shown. The stochastic variation between runs is small and is not visible in *A*. The fraction of platelet singlets that have aggregated in time is defined as $1 - N(1, t)/N(1, 0)$, where $N(1, t)$ is the concentration of platelet singlets at time $t$. Size distributions from the simulations are represented at the resolution of a Coulter counter with a 50-$\mu$m aperture (0.2 fl resolution) (*B*). The decrease in the height of the major peak is a consequence of the aggregation of platelet singlets undergoing homotypic aggregation in plasma levels of fibrinogen at $G = 335\ s^{-1}$ have a predicted half-life of 8.5 s.

In Fig. 3 *B* we present the size distributions of the aggregates resulting from type 1 simulations. The platelet volume distribution did not show peaks representing doublets, triplets, etc., but exhibited a subtle spreading to larger volumes as the peak height decreased in magnitude. The failure of the system to produce distinct peaks for each type of aggregate results from the concentration of platelets and the spread of the initial distribution. Initially, when such events are most likely to be directly observed, doublets were relatively rare in comparison to singlets and were hidden in the fluctuations of the overall size distribution. The shift in the mean aggregate volume was more visible in the normalized cumulative size distribution of the aggregates (Fig. 3 *C*). Whereas size distributions represent $N(u, t)$, the cumulative volume distribution $F$ is defined as $\Sigma_u^v N(u, t)/\Sigma_u N(u, t)$. As the aggregation progressed, the average aggregate volume shifted to the right and spread as expected. After 30 s, size states were distributed nonuniformly over three decades. The MC resolved size states with equal accuracy and resolution with remarkably small stochastic fluctuation.

Fig. 4 shows the analogous results for simulations of homotypic aggregation of fully activated neutrophils, using $\epsilon_{r+h}$ = 0.31 (Taylor et al., 1996; Tandon and Diamond, 1998). Simulations were carried out with an initial population of 12,000 singlets. In Fig. 4 *A*, the fraction of the neutrophils aggregated is shown. The half-life of fully activated neutrophil singlets was 2.0 s for $G = 335\ s^{-1}$. Owing to the initial size distribution of the neutrophils and their relative dilution in comparison with platelets, the volume distributions in Fig. 4 *B* show the appearance of distinct doublets and triplets. Consequently, these species should be observable in size distributions obtained in experimental aggregations. In fact, Neelamegham et al. (1997) clearly resolved 2-mers through 4-mers via autofluorescence of fixed neutrophils (a volumetric signal) analyzed by flow cytometry. These peaks in the size distribution cause distinct plateaus in the normalized cumulative distribution (Fig. 4 *C*). The rightward shift in aggregate volume with time was clear, and again, the MC simulation resolved the smallest and the largest volume states equally well.

In Fig. 5 we present the kinetic behavior of heterotypic aggregation of fully activated platelets and neutrophils at $G = 335\ s^{-1}$. This is the first report of simulation of heterotypic aggregation of platelets and neutrophils. The lack of measurement of heterotypic aggregation efficiencies is a direct result of the absence of a feasible solution method for the heterotypic PBE. We have formulated an estimate of

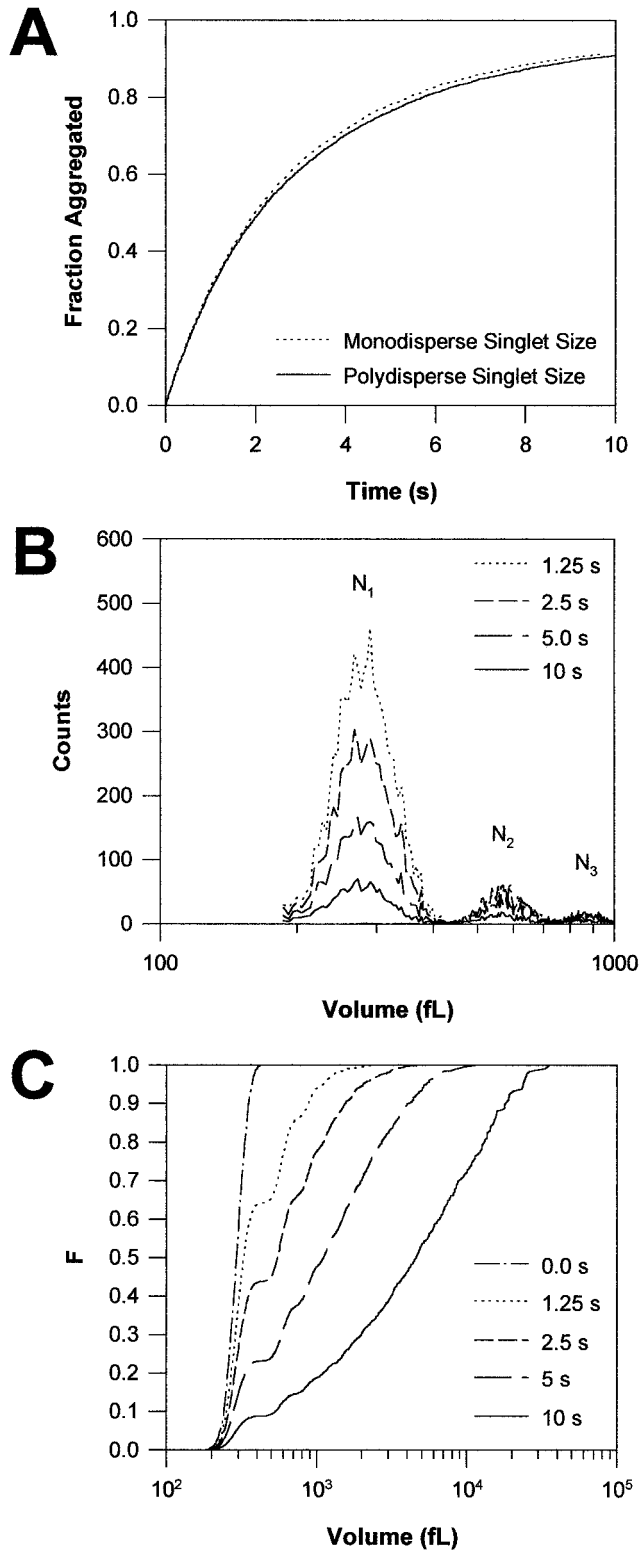


FIGURE 4 Behavior of the homotypic aggregation of fully activated neutrophils in a linear flow field of 335 $s^{-1}$ ($\epsilon_{r+h} = 0.31$ for 1 $\mu$M FMLP stimulated neutrophils aggregating via L-selectin, CD11a/CD18, and CD11b/CD18). The results of four simulations are shown (12,000 neutrophils/simulation). The fraction of neutrophil singlets that have aggregated is presented in *A*. Size distributions are represented at the resolution of a Coulter counter with a 100-$\mu$m aperture (4.5-fl resolution) (*B*). The decrease in the height of the major peak is a consequence of the aggregation of neutrophil singlets. The peaks to the right of the major peak represent doublets and triplets. The cumulative volume distribution *F* of neutrophil aggregates is presented in *C*.

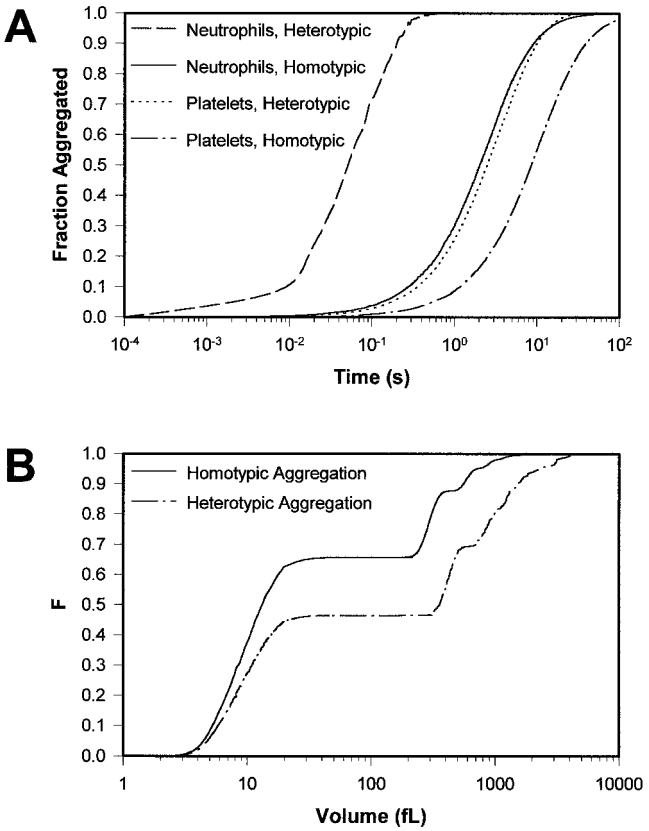


FIGURE 5 Consumption of fully activated platelets and neutrophils for heterotypic and homotypic aggregation conditions in a linear shear field of 335 $s^{-1}$ (*A*). When platelets and neutrophils interact, they aggregate much more quickly than when they aggregate independently. The half-life of platelets drops from 8.5 s to 2.4 s, and that of neutrophils drops from 2.4 s to 0.11 s, indicating that neutrophils sweep up platelets in large amounts in aggregating flow. The reduction in the half-life of platelets indicates that neutrophils participate in a nucleating mechanism to increase the speed of platelet aggregation. The cumulative volume distributions are shown after 1.25 s of cohomotypic aggregation of platelets and neutrophils (i.e., anti-P-selectin) and after 1.25 s of heterotypic aggregation (*B*). When the cells interact, the sizes of the aggregates increase by a factor of up to 4. Furthermore, not only are aggregates resulting from heterotypic aggregation larger, but the larger aggregates compose a greater fraction of the aggregates. For example, at 1.25 s, aggregates larger than 1000 fl compose only 2% of the aggregates in a cohomotypically aggregating mixture, but in a heterotypic aggregation, such aggregates constitute 20% of the particles.

the heterotypic kernel based upon experiments in the literature (see Appendix) to conduct our MC simulations of this phenomenon.

The adhesive interaction of the two cell types yielded dramatic effects: the half-lives of platelets and neutrophils dropped to 2.4 and 0.11 s, respectively, a 3.5-fold reduction for platelets and a 18-fold reduction for neutrophils. Further study showed that this is a population-driven phenomenon.

That is, the kernels $\beta(u, v, t)$ for homotypic aggregation of neutrophils ($u = v = 290.1$ fl) and heterotypic aggregation of platelets with neutrophils ($u = 290.1$ fl, $v = 7.68$ fl) have a ratio of 1.86, which suggests that homotypic aggregation is a more probable event than heterotypic aggregation. However, the weighting of the kernels in Eqs. 9 and 10 favors a heterotypic aggregation: for a system of 1,000 neutrophils and 60,000 platelets, there are only 500,500 combinations of neutrophils, whereas there are 60 million combinations of platelets with neutrophils. Thus combinatorial effects favor heterotypic aggregation by a factor of 120, outweighing the factor of 1.86 likelihood of homotypic aggregation based on kernels alone. Overall, heterotypic aggregation of neutrophils is favored by a factor of ~65 over homotypic aggregation.

Fig. 5 *B* compares the cohomotypic aggregation of platelets and neutrophils with their heterotypic aggregation at 1.25 s. When the two cell types do not interact (for example, if a blocking antibody is introduced against P-selectin or PSGL-1), the mean particle volume in cohomotypically aggregating medium is 13 fl, whereas the mean volume for heterotypically aggregating cells is 357 fl. Moreover, only 2% of the aggregates in a cohomotypic aggregation are larger than $10^3$ fl at 1.25 s, whereas 20% of those aggregating heterotypically fall in this range. Thus the heterotypic interaction between the two cell types not only promotes generation of more and larger aggregates, but promotes their rate of formation as well.

Fig. 5 illustrates the procoagulant effects of activated neutrophils for activated platelets (mediated by aggregation via P-selectin–PSGL-1 bonding, but independent of other biological effects, such as tissue factor expression or neutrophil Mac-1 binding of factor X). For example, consider a clotting episode near a wall ($G = 335\ s^{-1}$) where the shear field is approximately linear and the characteristic time of blood-wall interaction occurs during diastole (~0.5 s). Heterotypic aggregation causes the fraction of platelets aggregated to increase by nearly threefold from 0.05 to 0.14, and the fraction of neutrophils aggregated increases by eightfold from 0.15 to 1.0. Thus, anti-P-selectin antibodies, which are anti-thrombotic agents (Palabrica et al., 1992), may exert some of their effects under hemodynamic conditions to prevent neutrophil promotion of platelet accumulation.

We present the size-composition distributions of platelet-neutrophil aggregates in Fig. 6. The initial volume distributions of platelets and neutrophils used in all of our simulations are shown in Fig. 6 *A*. Composition distributions are shown at 0.01, 0.1, 1.0, 2.0, and 5.0 s (Fig. 6, *B–F*). Initially, heterotypic aggregation dominates, where neutrophils combine with only one or two platelets (Fig. 6 *B*). Because of the abundance of platelets, these aggregates increase their platelet content in the ensuing moments (Fig. 6 *C*). Aggregates with more than one neutrophil do not appear until almost all neutrophil singlets are consumed (Fig. 6 *D*). As in the homotypic aggregation of neutrophils, aggregates with distinct numbers of neutrophils form distinct regions in the composition distribution, whereas such regions do not occur for platelets. At later times, mass conservation limits the populations of aggregates, simultaneously decreasing the overall probabilities of aggregation and slowing down the aggregation process. Thus the slope of the spread of points is a result of the initial size distributions and populations of the cells.

Fig. 7 shows the kinetic behavior of species falling in two different volume gates (see Fig. 6 *B*). Here, Gate 1 includes all aggregates featuring 31–215 fl of platelets and 212–387 fl of neutrophils (1 fl = 1 $\mu m^3$). This corresponds to species with one neutrophil and 4–28 platelets. Gate 2 includes all aggregates featuring 130–514 fl of platelets and 450–730 fl of neutrophils (two neutrophils and 17–67 platelets). Using flow cytometry data in an experimental setting, a size- and composition-dependent aggregation kernel can be determined to match the dynamics, species distributions, and stochastic fluctuations seen in Figs. 6 and 7.

## DISCUSSION

The stochastic aggregation algorithm, based on species accounting, produced results remarkably precise in comparison with the discrete PBE (Eq. 1) solved analytically for three different ideal test kernels. The algorithm required less than 10 s of CPU time to run type 2 (volumetrically monodisperse singlets) simulations and less than 30 min to run type 1 (polydisperse) simulations when ~12,000 heterotypic singlets were simulated.

For the first time, heterotypic aggregation of platelets and neutrophils (neglecting fragmentation) was simulated for a realistic kernel estimated from experiments on homotypic aggregations of these cells. During heterotypic aggregation in a linear shear field, platelets behaved like an excess reagent in a chemical reaction, used for driving the conversion of another reagent. In this case, the limiting reagent is the neutrophil, which also serves as a catalyst for platelet consumption because of its large sweep through space. Activated neutrophils serve as nucleation sites for heterotypic aggregation of platelets and other neutrophils and are prothrombotic because of their aggregation biophysics as well as their biochemistry (Palabrica et al., 1992; Plescia and Altieri, 1996). Our theoretical prediction is in line with the observations of Bednar et al. (1985), who observed a decrease in platelet accumulation in infarcted myocardium when neutrophils were depleted. The hemodynamics and receptor biophysics of blood coagulation can be studied more precisely now that aggregation kernels can be deconvoluted from heterotypic aggregation experiments.

The stochastic aggregation algorithm has predictive power for any type of aggregation, regardless of the number of types of monomers, or whether they vary in volume. However, our approach is not the only one capable of handling complicated aggregation spaces. Other stochastic aggregation algorithms are available (Gillespie, 1975; Shah et al., 1977; Smith and Matsoukas, 1998), of which the fastest is the full conditioning method (Gillespie, 1975),

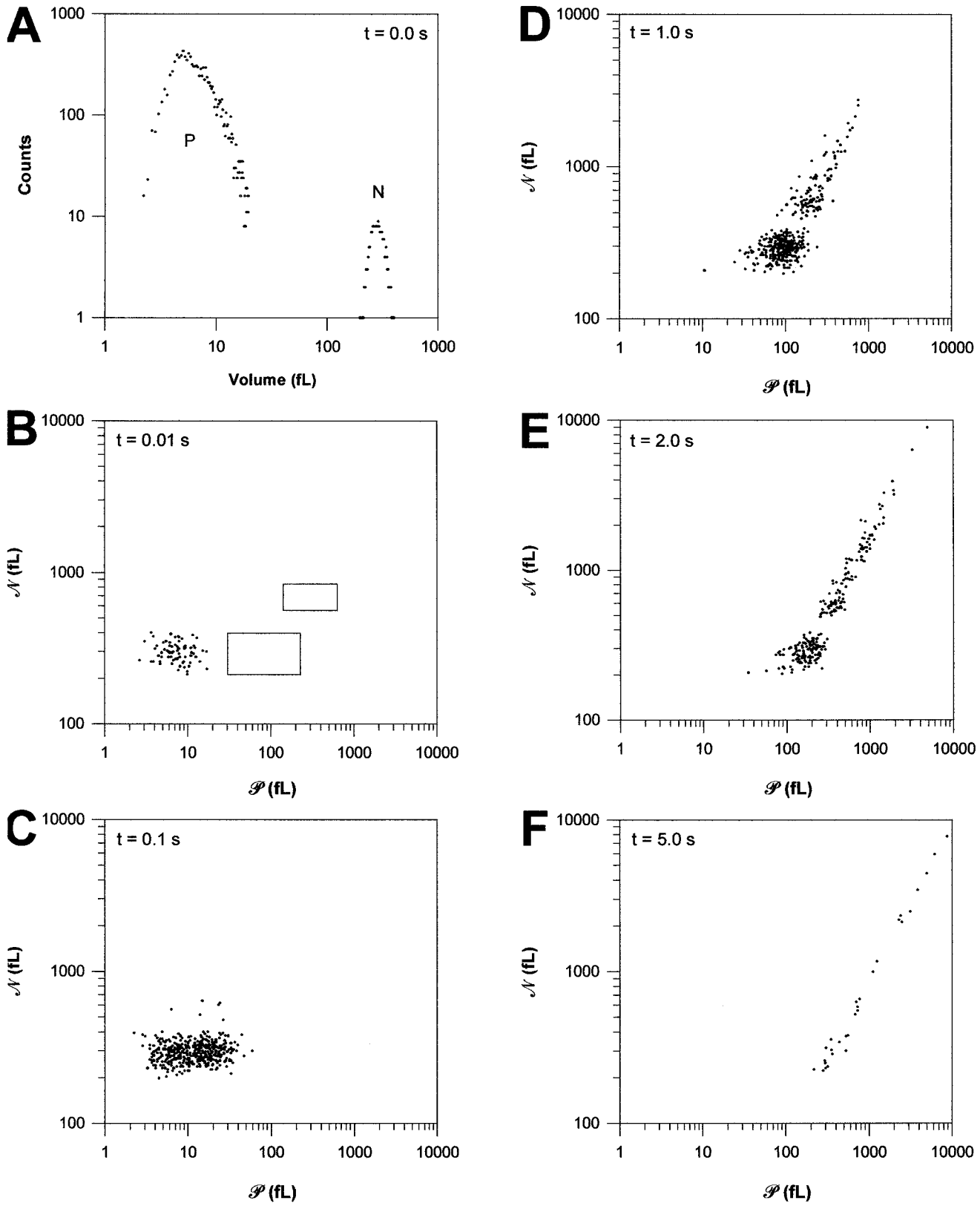


FIGURE 6 Size and composition distributions of platelet-neutrophil aggregates formed at 335 $s^{-1}$ with full cellular activation. The initial volume distributions of platelets and neutrophils are given in *A*. Composition distributions of aggregates are given for 0.01 s (*B*), 0.1 s (*C*), 1.0 s (*D*), 2.0 s (*E*), 5.0 s (*F*). The axes represent the volume content of platelets and neutrophils within the aggregates represented (1 fl = 1 $\mu m^3$). Because of the combinatorial disadvantage of doublet formation of neutrophils in this aggregation mixture, neutrophil doublets never appear alone, but are always stuck to platelets, which mediate their adhesion. As in Figs. 3 *B* and 4 *B*, whereas neutrophil doublets, triplets, etc. are easily distinguished, those of platelets are indistinguishable. The gates of Fig. 7 are shown in *B*.

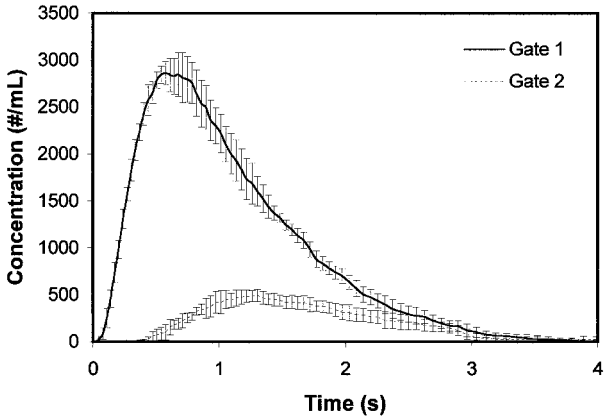


FIGURE 7 Evolution of aggregates within specific platelet and neutrophil volume gates. The series labeled Gate 1 represents aggregates with one neutrophil and ~4–28 platelets. Gate 2 features aggregates with two neutrophils and ~17–67 platelets. Because they represent dozens of stochastically varying species, the variation in the concentrations of these "gated species" is notable, whereas the concentrations of platelet singlets (Fig. 3 *A*) and neutrophil singlets (Fig. 4 *A*) have small standard deviations between runs. Gates 1 and 2 are shown in Fig. 6 *B*.

which employs particle accounting. For a system with $\omega$ particles, it requires calculations of $\omega(\omega - 1)/2$ kernels before it can proceed to the next time step. When the kernel is not a function of time, this may be reduced to $\omega$ kernel calculations. Thus, for time-independent kernels, the full conditioning method requires $O(\Omega)$ kernel calculations per time step, where $\Omega$ is the initial number of monomers, given monodisperse initial conditions. However, as our MC algorithm employs species accounting, only $m$ kernels need be computed per time step, where $m$ is the number of species. Given that the maximum number of species occurs when there is only one of each, the mass balance gives the following:

$$1 + 2 + 3 + \cdots + m = \tfrac{1}{2}m(m + 1) = \Omega \qquad (29)$$

Thus, in this "worst case" distribution, we see that $m \approx (2\Omega)^{1/2}$. In both real and model aggregations such as those simulated, such a complete distribution across the species space does not occur. The actual distribution across the species space is a function of time and depends on the form of the kernel. Thus the number of kernel calculations per time step is a small fraction of $\Omega^{1/2}$. Still, for comparative purposes, each time step in our algorithm requires $O(\Omega^{1/2})$ kernel calculations, a significant improvement over the full conditioning method.

The kernel can change with time when aggregating cells up-regulate, down-regulate, or shed receptors as they react to external or internal stimuli. In such cases, our algorithm becomes less efficient; all $c(i, j, t)$ must be recalculated at every time step, increasing the number of kernel calculations from $m$ to $m + m(m - 1)/2! = \frac{1}{2}m(m + 1)$. Thus, considering Eq. 29, our algorithm requires $O(\Omega)$ kernel calculations per time step when the kernel changes with time. This is still better than the full conditioning method, which in this situation is forced to calculate $O(\Omega^2)$ kernels per time step, because every particle-particle interaction must be examined. In practice, it may not be necessary to recalculate the kernels at every time step if they change slowly over the course of aggregation.

There are relevant practical details to note when running simulations with this method. In homotypic aggregation with species defined by the number of monomers, the index of a species in a list can be used to denote the number of monomers in that species, simplifying the bookkeeping. However, when heterotypic aggregation is simulated, the numbers or amounts of each cell type must be accounted for when new species are created. Moreover, for any system where the volume or set of subvolumes of a particle defines its species, the volumes of each cell type in each species must be considered when new species are created. Consequently, a location in a list is insufficient to specify the volume or composition of a species. Thus, to account for the size and composition of each species properly, the numbers or volumes of platelets and neutrophils should be maintained in arrays parallel to the species index array, and a bookkeeping matrix containing pointers should be used to specify species composition. Taking these measures prevents the redundant generation of an existing species during the simulation. For a system of $\mathcal{D}$ types of monomers, $\mathcal{D}$ parallel arrays will be required for these tasks. This is general for simulations of aggregation of particles of discrete and continuously varying volume. Fortunately, these are not computationally intensive, as they will be low-memory integer variables that are not used directly in computation. The computationally slow step remains the calculation of new kernels.

When run on a Sun Ultra 30 or Silicon Graphics $O_2$, type 1 simulations of heterotypic aggregation required 4–30 min to run, depending on the number of particles simulated. Type 2 simulations required 4 s at most. Because of the complexity of the initial conditions, $O(1000)$ species were generated during the course of aggregation. Equivalent expression of the system through a PBE such as Eq. 1 would require ~1000 differential equations with ~750 terms on average. The method of Hounslow et al. (1988) discretizes the integral in Eq. 6 to conserve mass and integrates the resulting equations by finite difference. However, with only 30 volume bins, it still requires more than 2 h of CPU time to simulate homotypic platelet aggregation. Furthermore, unlike our method, the Hounslow method requires several approximations: approximation of an infinitesimal d$t$ as a finite $\Delta t$, substantial simplification in species space through the volume discretization, and the assumption that aggregation can be described as a deterministic process.

Although the stochastic aggregation algorithm is exact for bulk aggregation, it must be modified for complicated aggregation media with spatial gradients. That is, if the likelihood of an aggregation is strongly dependent on the absolute rather than relative positions of the aggregating particles, $P(\tau, \mu)$ must be replaced with $P(\tau, \mu, \mathbf{r})$, where $\mathbf{r}$ specifies the location of an aggregation event. For example,

in arteries, shear rate varies with radial position, and aggregation events are coupled with deposition at the wall. In such cases, position would be a complicated and nontrivial factor to account for in MC simulation.

In addition to providing a new tool that permits feasible prediction of the behavior of both heterotypic and homotypic aggregation, the stochastic aggregation algorithm also makes amenable the inverse problem. That is, iterative fitting of kernels to experimental data such as flow cytometry and Coulter counter distributions will allow direct deconvolution of size- and composition-dependent kernels. From these, receptor bonding rate constants may be estimated, because kernels depend on shear rate, aggregate sizes, receptor concentrations, and receptor on-rates and off-rates (Bell, 1981; Tandon and Diamond, 1997, 1998; Long et al., 1999). Iterative solution for these parameters is finally possible for heterotypic aggregation between cells, colloids, polymers, proteins, and other aggregating media. Such methods may detect and quantify subtle changes in human blood that are diagnostic of clinical states or help define the pharmacological-hemodynamic performance of blood.

## APPENDIX: MODELING THE HETEROTYPIC AGGREGATION OF PLATELETS AND NEUTROPHILS

At $G = 335\ s^{-1}$, the overall efficiencies $\epsilon_{r+h}$ for homotypic aggregations of platelets and neutrophils in plasma are 0.05 and 0.31, respectively (Bell et al., 1989a,b; Taylor et al., 1996; Tandon and Diamond, 1997, 1998). Because of the complexity of the aggregation space, experimentally determined efficiencies for the heterotypic aggregation of platelets and neutrophils are not available. In the present study, we approximated this efficiency, $\epsilon_{r+h}(\mathcal{P}_i, \mathcal{N}_i, \mathcal{P}_j, \mathcal{N}_j, G)$, to be a function of the platelet volume fractions $y_i = \mathcal{P}_i/(\mathcal{P}_i + \mathcal{N}_i)$ alone. Then, drawing from the fact that $\epsilon_{r+h}(y_i, y_j) = \epsilon_{r+h}(y_j, y_i)$, the efficiency was expressed in terms of a single variable, $s = (y_i^2 + y_j^2)^{1/2}$.

The data in Figs. 3–7 were generated using the following functional form for $\epsilon_{r+h}(s, G = 335\ s^{-1})$:

$$\epsilon_{r+h}(s) = C_1 s^2 + C_2 s + C_3 \qquad \text{(A1)}$$

where

$$C_1 = -(1 + \sqrt{2})\epsilon_{\text{plat-neut}} + \frac{\sqrt{2}}{2}\epsilon_{\text{neut}} + \epsilon_{\text{plat}} = -1.20$$

$$C_2 = \frac{2\epsilon_{\text{plat-neut}} - \epsilon_{\text{neut}} - \epsilon_{\text{plat}}}{2 - \sqrt{2}} = 1.47$$

$$C_3 = \epsilon_{\text{neut}} = 0.31$$

The coefficients $C_1$, $C_2$, and $C_3$ fit the experimentally determined values of $\epsilon_{r+h}$ for the homotypic aggregations of platelets ($s = \sqrt{2}$) and neutrophils ($s = 0$). They are also fitted to the estimated efficiency for the heterotypic aggregation of platelet and neutrophil singlets, $\epsilon_{\text{plat-neut}}$. Because of the large number of fast and strong receptor-ligand interactions between platelets and neutrophils in plasma (PSGL-1–P-Selectin, Mac-I–fibrinogen–GPIIb/IIIa, and LFA-1–ICAM-2), fully activated platelets and neutrophils should aggregate upon collision ($\epsilon_r = 1$). Thus the value of $\epsilon_{\text{plat-neut}}$ was approximated as the average hydrodynamic efficiency, 0.61 (Tandon and Diamond, 1998), which simply corrects the Smoluchowski kernel for curvilinear trajectories of particles in viscous flow. In this study, we have not explicitly accounted for the variation of the efficiency with the size ratio of the colliding particles, taking such effects as lumped within the experimentally determined efficiencies. Accounting for such size effects would have a small effect on the speed of the MC algorithm to the extent that it would increase the computation time for the coagulation kernel.

This work was supported by National Institutes of Health grant HL 56621 and National American Heart Association grant 96-6670. SLD is an Established Investigator of the National American Heart Association.

## REFERENCES

Bednar, M., B. Smith, A. Pinto, and K. M. Mullane. 1985. Neutrophil depletion suppresses $^{111}$In-labeled platelet accumulation in infarcted myocardium. *J. Cardiovasc. Pharmacol.* 7:906–912.

Bell, G. I. 1979. A theoretical model for adhesion between cells mediated by multivalent ligands. *Cell Biophys.* 1:133–147.

Bell, G. I. 1981. Estimate of the sticking probability for cells in uniform shear flow with adhesion caused by specific bonds. *Cell Biophys.* 3:289–304.

Bell, D. N., S. Spain, and H. L. Goldsmith. 1989a. Adenosine diphosphate induced aggregation of human platelets in flow through tubes. I. Measurement of concentration and size of single platelets and aggregates. *Biophys. J.* 56:817–828.

Bell, D. N., S. Spain, and H. L. Goldsmith. 1989a. Adenosine diphosphate induced aggregation of human platelets in flow through tubes. II. Effect of shear rate, donor sex, and ADP concentration. *Biophys. J.* 56: 817–828.

Belval, T. K., and J. D. Hellums. 1986. Analysis of shear induced platelet aggregation with population balance mathematics. *Biophys. J.* 50: 479–487.

Brown, K. K., P. M. Henson, J. Maclouf, M. Moyle, J. A. Ely, and G. S. Worthen. 1998. Neutrophil-platelet adhesion: relative roles of platelet P-selectin and neutrophil $\beta 2$ (CD18) integrins. *Am. J. Respir. Cell. Mol. Biol.* 18:100–110.

Delisi, C. 1980. Theory of clustering of cell surface receptors by ligands of arbitrary valence: dependence of dose response patterns on a coarse cluster characteristic. *Math. Biosci.* 52:159–184.

Elizalde, I., J. Gomez, J. Panes, M. Lozano, M. Casadevall, J. Ramirez, P. Pizcueta, F. Marco, F. D. deRojas, D. N. Granger, and J. M. Pique. 1997. Platelet activation in mice and human *Helicobacter pylori* infection. *J. Clin. Invest.* 100:996–1005.

Evangelista, V., S. Manarini, S. Rotondo, N. Martelli, R. Polischuk, J. L. McGregor, G. deGaetano, and C. Cerletti. 1996. Platelet/polymorphonuclear leukocyte interaction in dynamic conditions: evidence of adhesion cascade and cross talk between P-selectin and the beta 2 integrin CD11b/CD18. *Blood.* 88:4183–4194.

Gillespie, D. T. 1972. The stochastic coalescence model for cloud droplet growth. *J. Atmos. Sci.* 29:1496–1510.

Gillespie, D. T. 1975. An exact method for numerically simulating the stochastic coalescence process in a cloud. *J. Atmos. Sci.* 32:1977–1989.

Gillespie, D. T. 1976. A general method for numerically simulating the stochastic time evolution of coupled chemical reactions. *J. Comput. Phys.* 22:403–434.

Gillespie, D. T. 1977. Exact stochastic simulation of coupled chemical reactions. *J. Phys. Chem.* 81:2340–2361.

Hamburger, S. A., and R. P. McEver. 1990. GMP-140 mediates adhesion of stimulated platelets to neutrophils. *Blood.* 75:550–554.

Hounslow, M. J., R. L. Ryall, and V. R. Marshall. 1988. A discretized population balance for nucleation, growth, and aggregation. *AIChE J.* 34:1821–1832.

Huang, P. Y., and J. D. Hellums. 1993a. Aggregation and disaggregation kinetics of human blood platelets. I. Development and validation of a population balance method. *Biophys. J.* 65:334–343.

Huang, P. Y., and J. D. Hellums. 1993b. Aggregation and disaggregation kinetics of human blood platelets. II. Shear-induced platelet aggregation. *Biophys. J.* 65:344–353.

Huang, P. Y., and J. D. Hellums. 1993c. Aggregation and disaggregation kinetics of human blood platelets. III. Disaggregation under shear stress of platelet aggregation. *Biophys. J.* 65:354–361.

Konstantopoulos, K., S. Neelamegham, A. R. Burns, E. Hentzen, G. S. Kansas, K. R. Snapp, E. L. Berg, J. D. Hellums, C. W. Smith, L. V. McIntire, and S. I. Simon. 1998. Venous levels of shear support neutrophil-platelet adhesion and neutrophil aggregation in blood via P-selectin and beta(2)-integrin. *Circulation.* 98:873–882.

Long, M., H. L. Goldsmith, D. F. J. Tees, and C. Zhu. 1999. Probabilistic modeling of shear-induced formation and breakage of doublets cross-linked by receptor-ligand bonds. *Biophys. J.* 76:1112–1128.

Macken, C. A., and A. S. Perelson. 1982. Aggregation of cell surface receptors by multivalent ligands. *J. Math. Biol.* 14:365–370.

Minamino, T., M. Kitakaze, H. Asanuma, Y. Tomiyama, M. Shiraga, H. Sato, Y. Ueda, H. Funaya, T. Kuzuya, K. Matsuzawa, and M. Hori. 1998. Endogenous adenosine inhibits P-selectin-dependent formation of coronary thromboemboli during hypoperfusion in dogs. *J. Clin. Invest.* 101:1643–1653.

Neelamegham, S., A. D. Taylor, J. D. Hellums, M. Dembo, C. W. Smith, and C. I. Simon. 1997. Modeling the reversible kinetics of neutrophil aggregation under hydrodynamic shear. *Biophys. J.* 72:1527–1540.

Neelamegham, S., and K. Zygourakis. 1997. A quantitative assay for intercellular aggregation. *Ann. Biomed. Eng.* 23:180–189.

Neumann, F. J., N. Marx, M. Gawaz, K. Brand, I. Ott, C. Rokitta, C. Sticherling, C. Meinl, A. May, and A. Schomig. 1997. Induction of cytokine expression in leukocytes by binding of thrombin-stimulated platelets. *Circulation.* 95:2387–2394.

Ott, I., F. J. Neumann, M. Gawaz, M. Schmitt, and A. Schomig. 1996. Increased neutrophil-platelet adhesion in patients with unstable angina. *Circulation.* 94:1239–1246.

Palabrica, T., R. Lobb, B. C. Furie, M. Aronovitz, C. Benjamin, Y. M. Hsu, S. A. Sajer, and B. Furie. 1992. Leukocyte accumulation promoting fibrin deposition is mediated in vivo by P-selectin on adherent platelets. *Nature.* 359:848–851.

Perelson, A. S. 1981. Receptor clustering on cell surface. III. Theory of receptor crosslinking by multivalent ligands: description by ligand states. *Math. Biosci.* 53:1–39.

Perelson, A. S., and F. W. Wiegel. 1982. The equilibrium size distribution of rouleaux. *Biophys. J.* 37:515–522.

Plescia, J., and D. C. Altieri. 1996. Activation of Mac-1 (CD11b/CD18)-bound factor X by released cathepsin G defines an alternative pathway of leucocyte initiation of coagulation. *Biochem. J.* 319:873–879.

Ponder, E. 1927. On sedimentation and rouleau formation. II. *Q. J. Exp. Physiol.* 16:173–194.

Ramkrishna, D. 1973. A puristic analysis of population balance. I. *Chem. Eng. Sci.* 28:1423–1435.

Rinder, H. M., J. L. Bonan, C. S. Rinder, K. A. Ault, and B. R. Smith. 1991. Activated and unactivated platelet adhesion to monocytes and neutrophils. *Blood.* 78:1760–1769.

Rinder, C. S., J. L. Bonan, H. M. Rinder, J. Matthew, R. Hines, and B. R. Smith. 1992. Cardiopulmonary bypass induces leukocyte-platelet adhesion. *Blood.* 79:1201–1205.

Samsel, R. W., and A. S. Perelson. 1982. The kinetics of rouleau formation. *Biophys. J.* 37:493–514.

Scott, W. T. 1965. Analytical studies of cloud droplet coalescence I. DRI Technical Report 9. University of Nevada, Reno, NV.

Shah, B. H., D. Ramkrishna, and J. D. Borwanker. 1977. Simulation of particulate systems using the concept of the interval of quiescence. *AIChE J.* 23:897–904.

Smith, M., and T. Matsoukas. 1998. Constant-number Monte Carlo simulation of population balances. *Chem. Eng. Sci.* 53:1777–1786.

Smoluchowski, M. v. 1917. Vensuch einer mathematischen theorie der koagulation kinetic kolloider losungen. *Z. Phys. Chem.* 92:129–168.

Tandon, P., and S. L. Diamond. 1997. Hydrodynamic effects and receptor interactions of platelets and their aggregates in linear shear flow. *Biophys. J.* 73:2819–2835.

Tandon, P., and S. L. Diamond. 1998. Kinetics of $\beta_2$-integrin and L-selectin bonding during neutrophil aggregation in shear flow. *Biophys. J.* 75:3163–3175.

Taylor, A. D., S. Neelamegham, J. D. Hellums, C. W. Smith, and S. I. Simon. 1996. Molecular dynamics of the transition from L-selectin to $\beta_2$-integrin dependent neutrophil adhesion under defined hydrodynamic shear. *Biophys. J.* 71:3488–3500.

Von Schulthess, G., B. Benedek, and R. W. De Blois. 1983. Experimental measurements of the temporal evolution of cluster size distributions for higher functionality antigens cross-linked by antibody. *Macromolecules.* 16:434–440.